Physiol Genomics 53: 358–371, 2021.
First published July 12, 2021; doi:10.1152/physiolgenomics.00001.2021

american physiological society | PHYSIOLOGICAL GENOMICS

RESEARCH ARTICLE

Chronic binge alcohol and ovariectomy dysregulate omental adipose tissue metaboproteome in simian immunodeficiency virus-infected female macaques

Jonquil M. Poret,[1,2] Jessie J. Guidry,[3] Liz Simon,[1,2] and Patricia E. Molina[1,2]

[1]*Department of Physiology, Louisiana State University Health Sciences Center, New Orleans, Louisiana;* [2]*Comprehensive Alcohol-HIV/AIDS Research Center, Louisiana State University Health Sciences Center, New Orleans, Louisiana; and* [3]*Department of Biochemistry and The Proteomic Core Facility, Louisiana State University Health Sciences Center, New Orleans, Louisiana*

Abstract

Effective antiretroviral therapy (ART) has significantly reduced mortality of people living with HIV (PLWH), and the prevalence of at-risk alcohol use is higher among PLWH. Increased survival and aging of PLWH is associated with increased prevalence of metabolic comorbidities especially among menopausal women, and adipose tissue metabolic dysregulation may be a significant contributing factor. We examined the differential effects of chronic binge alcohol (CBA) administration and ovariectomy (OVX) on the omental adipose tissue (OmAT) proteome in a subset of simian immunodeficiency virus (SIV)-infected macaques of a longitudinal parent study. Quantitative discovery-based proteomics identified 1,429 differentially expressed proteins. Ingenuity Pathway Analysis (IPA) was used to calculate *z*-scores, or activation predictions, for functional pathways and diseases. Results revealed that protein changes associated with functional pathways centered around the "OmAT metaboproteome profile." Based on *z*-scores, CBA did not affect functional pathways of metabolic disease but dysregulated proteins involved in adenosine monophosphate-activated protein kinase (AMPK) signaling and lipid metabolism. OVX-mediated proteome changes were predicted to promote pathways involved in glucose- and lipid-associated metabolic disease. Proteins involved in apoptosis, necrosis, and reactive oxygen species (ROS) pathways were also predicted to be activated by OVX and these were predicted to be inhibited by CBA. These results provide evidence for the role of ovarian hormone loss in mediating OmAT metaboproteome dysregulation in SIV and suggest that CBA modifies OVX-associated changes. In the context of OVX, CBA administration produced larger metabolic and cellular effects, which we speculate may reflect a protective role of estrogen against CBA-mediated adipose tissue injury in female SIV-infected macaques.

adipose; alcohol; ovariectomy; proteomics; SIV

INTRODUCTION

Of the estimated 1.2 million people living with HIV (PLWH) in the United States, ~50% are 50 yr of age or older and women account for more than half of this population (1). With increased survival and aging of PLWH on antiretroviral therapy (ART), the incidence of comorbid conditions such as metabolic dysregulation (2, 3) and early onset menopause in HIV-infected women (4, 5) is increased and exceeds that of the general population. At-risk alcohol consumption is common among PLWH (6–8) and is associated with accelerated disease progression/severity and increased development of metabolic comorbidities in both PLWH and a preclinical model of simian immunodeficiency virus (SIV) infection (9–15).

Adipose tissue dysregulation is a central mechanism mediating metabolic comorbidities among PLWH (16–20). In fact, at-risk alcohol use, HIV/ART, and aging, especially among postmenopausal women, have been shown to independently produce similar negative effects on adipose tissue biology, function, and overall metabolic health. At-risk alcohol use impairs adipose tissue lipid metabolism and glucose tolerance, particularly in visceral adipose tissue (21–23), alters adipokine secretion (24, 25), and increases risk for metabolic disease (26–28). HIV/ART contributes to alterations in adipose tissue distribution, including increased visceral/abdominal adiposity (18, 19, 29), impaired adipogenesis (29–31), disrupted adipokine release (32, 33), increased adipose inflammation, and reduced insulin sensitivity (32–34). Postmenopausal status is associated with increased visceral adiposity (35), impaired adipose tissue lipid and carbohydrate metabolism (36, 37), lowered adiponectin (38), and an increased risk for metabolic syndrome (39, 40). Preclinical models of ovarian hormone loss have shown that loss of estrogen disrupts insulin signaling protein expression and promotes adipose inflammation (41), increases adipocyte lipid accumulation (42), and promotes adipose tissue hypertrophy, hyperplasia, and glucose intolerance (43). Despite several studies providing evidence for similar negative impacts, very few studies have

Correspondence: P. E. Molina (pmolin@lsuhsc.edu).
Submitted 4 January 2021 / Revised 19 May 2021 / Accepted 18 June 2021

investigated the combined effects of alcohol, HIV/ART, and/or postmenopausal status on adipose tissue biology and metabolic health.

The rhesus macaque SIV model is an established and highly relevant preclinical animal model for investigating the pathophysiological consequences of chronic alcohol in the context of immunodeficiency virus infection. Previous studies from our laboratory have shown that chronic binge alcohol (CBA) administration leads to marked dysregulation of glucose-insulin dynamics and accentuates metabolic derangements in SIV infection (13, 44, 45). CBA administration reduced serum adiponectin, an insulin-sensitizing adipokine, omental adipocyte cell size, and in vitro adipogenic differentiation ability of adipose-derived stem cells, whereas increasing omental adipose collagen expression in male SIV-infected, ART-treated rhesus macaques (44, 45). Taken together, these findings strongly suggest that CBA accelerates whole body and organ-specific metabolic dysfunction, especially of adipose tissue, in SIV-infected, ART-treated macaques.

Much of the knowledge of alcohol-mediated effects on adipose tissue was acquired in HIV-negative models or male PLWH, thus the effects of CBA on adipose tissue health in a HIV-infected host and how these effects are influenced by loss of ovarian hormones is largely under investigated. Visceral adiposity, which is associated with increased mortality in PLWH, is also associated with the development of metabolic disorders including dyslipidemia, insulin resistance, and impaired glucose homeostasis (46–50). Using a relevant preclinical model of HIV and proteomic analysis, the goal of this study was to examine the differential effects of CBA administration and ovarian hormone loss, simulated by ovariectomy (OVX), on the omental adipose tissue (OmAT) proteome of SIV-infected, ART-treated female rhesus macaques. Proteins are the executors of most physiological processes and functions. Quantitative proteomic analysis is a reliable and powerful experimental approach used for global differential analysis of proteins. Quantitative proteomics provides insight into the molecular framework and physiology of biological samples, processes, and disease states. By focusing on the differential protein expression of OmAT, we hope to bridge the gap and provide more understanding of overall biological processes and functions that are dysregulated due to alcohol and/or OVX in SIV.

METHODS

Animal Experiments

All experiments described in this study were approved by the Institutional Animal Care and Use Committee at Louisiana State University Health Sciences Center (LSUHSC, New Orleans, LA) and adhered to the National Institutes of Health guidelines for the care and use of experimental animals. The pathophysiological course of SIV infection has been previously described in published manuscripts using male rhesus macaques (13, 51–55). This is the first report of findings in the adipose tissue of SIV-infected, ART-treated female rhesus macaques.

OmAT samples used in the present study were obtained from a subset of macaques included in an ongoing parent longitudinal study. For this study, proteomic analysis was performed on OmAT of 16 macaques. The experimental design of the parent study is described below.

Adult (6- to 9-yr-old) female Indian rhesus macaques (*Macaca mulatta*) were randomized to either (1) chronic binge alcohol-administered (CBA) or (2) isovolumetric water-administered (VEH) groups. Animals were surgically implanted with gastric catheters and administered alcohol at a concentration of 30% (wt/vol) in water (30 min infusion; 13–14 g/kg/wk of alcohol; 5 days/wk). Macaques achieved a peak blood alcohol level of 50–60 mM (~230 mg%), 2 h after alcohol initiation. After 3 mo of CBA or VEH administration, animals were infected intravaginally with SIV_{mac251}. At 2.5 mo post-SIV infection, coinciding with viral set-point, all animals were initiated on daily subcutaneous injections of 20 mg/kg of Tenofovir {TFV, 9-[2-(phosphonomethoxy) propyl] adenine, PMPA} and 30 mg/kg of emtricitabine (FTC), provided by Gilead Sciences Inc. (Foster City, CA). This dose and drug combination effectively suppresses viral load and results in minimal toxicity in normal healthy macaques from infancy to adulthood and does not result in liver or renal toxicity in SIV-infected macaques (54). One month postinitiation of ART, animals were randomized to either ovariectomy (OVX) or sham (SHAM) surgery for a total of four treatment groups: VEH-SHAM (n = 4), VEH-OVX (n = 5), CBA-SHAM (n = 4), and CBA-OVX (n = 3). Eight months following OVX or sham surgery, after an overnight fast, all macaques were euthanized according to the American Veterinary Medical Association's guidelines. Each SIV-infected rhesus macaque was euthanized by first anesthetizing the animal with ketamine xylazine (10 mg/kg). Buprenex is administered via intravenous catheter and undiluted propofol is administered slowly intravenously at 1–2 mg/kg to effect induction of anesthesia with a maintenance infusion rate of 24–37 mg/kg/h throughout the perfusion procedure. Perfusion is achieved for 2–5 min using ice-cold Ringer's solution administered using a perfusion/embalming machine. After the perfusion, death is confirmed with intravenous administration of pentobarbital (1.8–10 mg/kg). Euthanasia before study-end was performed as needed based on the presence of any one of the following criteria: loss of 25% of body weight, complete anorexia for 4 days, major organ failure, or medical conditions unresponsive to treatment and surgical complications unresponsive to immediate intervention. OmAT samples were excised at necropsy and immediately flash frozen for further analysis. The total time for CBA or VEH administration was 14.5 mo, SIV infection for 11.5 mo, and 9 mo on ART.

Anthropometric Measurements

Body weight was recorded weekly using an Avery Weigh-Tronix scale with a WI-125 electronic weight indicator. Crown-rump length was measured with the macaque lying on its side, shoulder line vertically perpendicular to the body from the top of the unflexed head to the junction of the rump-tail groove. Body mass index (BMI) was calculated as kg of body/m^2 of crown rump length.

Body Composition

Dual-energy X-ray absorptiometry scans were performed to assess total body lean and fat mass Prodigy Total Body Fan-Beam densitometer (GE Medical Systems, Madison, WI)

with a Small Animal Package of the enCORE software was used for the measurements.

Protein Preparation for Discovery-Based Quantitative Shotgun Proteomics

Protein was isolated from OmAT samples by the addition of 1% SDS and sonication. Protein concentration was determined using a BCA Protein Assay Kit (Thermo Fisher Scientific, Waltham, MA). Based on the protein concentration, 100 μg of each sample was prepared for trypsin digestion by reducing the cysteines with tris(2-carboxyethyl) phosphine (TCEP) followed by alkylation with iodoacetamide (IAA). After chloroform-methanol precipitation, each protein pellet was digested with trypsin overnight at 37°C. The digested product was labeled using a tandem mass tag (TMTpro) 16-Plex Reagent Set (Thermo Fisher Scientific) according to the manufacturer's protocol, and following a hydroxylamine quench, was stored at −80°C until further use.

An equal amount of each TMT prolabeled sample was pooled together in a single tube and SepPak purified (Waters Chromatography, Dublin, Ireland) using acidic reverse phase conditions. To eliminate unreacted TMTpro, a 10% acetonitrile (ACN) wash was performed before elution of labeled peptides in 70% ACN. After complete drying, an off-line fractionation step was used to reduce sample complexity. The sample was resuspended in 10 mM ammonium hydroxide, pH 10. This mixture was subjected to basic pH reversed-phase chromatography (Dionex UltiMate 3000; Thermo Fisher Scientific). Briefly, the fractions were ultraviolet (UV) monitored at 215 nm for an injection of 100 μL at 0.1 mL/min with a gradient developed from 10 mM ammonium hydroxide (pH = 10) to 100% ACN over 90 min. A total of 48 fractions (200 μL each) were collected in a 96-well microplate and recombined in a checkerboard fashion to create 16 "superfractions" (original fractions 1, 17, and 33 became new superfraction #1, etc.; original fractions 2, 18, and 34 became new superfraction #2, etc.) (56).

The 16 superfractions were then analyzed on a Dionex UltiMate 3000 nano-flow system (LC) coupled to a Thermo Fisher Scientific Orbitrap Fusion Tribrid mass spectrometer (MS). Each fraction was subjected to a 90-min chromatographic method employing a gradient from 2% to 25% ACN in 0.1% formic acid (ACN/FA) over the course of 65 min, a gradient to 50% ACN/FA for an additional 10 min, a step to 90% ACN/FA for 5 min, and a 10-min re-equilibration into 2% ACN/FA. Chromatography was carried out in a "trap-and-load" format using an EASY-Spray source (Thermo Fisher Scientific); trap column C18 PepMap 100, 5 μm, 100 A and the separation column was EASY-Spray PepMap RSLC C18, 2 μm, 100 A, 25 cm. The entire run was at a flow rate of 0.3 μL/min and electrospray was achieved at 1.8 kV.

TMTpro data acquisition utilized an MS3 approach for data collection (57). Survey scans (MS1) were performed in the Orbitrap utilizing a resolution of 120,000. Data-dependent scans (MS2) were performed in the linear ion trap using a collision-induced dissociation of 25%. Reporter ions were fragmented using high-energy collision dissociation (HCD) of 65% and detected in the Orbitrap using a resolution of 50,000. This was repeated for a total of five technical replicates.

Bioinformatic and Principal Component Analyses

TMTpro data analysis was performed using Proteome Discoverer 2.3 (Thermo Fisher Scientific) (58–61). Each run of the 16 "superfractions" was merged and searched using SEQUEST HT (62). The Protein FASTA database was *Macaca mulatta*, SwissProt, Tax ID = 9544, version 2018-10-25 and contained 44,389 protein sequences. Static modifications included TMTpro reagents on lysine and *N*-terminus (+304.2071), carbamidomethyl on cysteines (+57.021), and dynamic modification of oxidation of methionine (+15.9949). Parent ion tolerance was 10 ppm, fragment mass tolerance was 0.6 Da, and the maximum number of missed cleavages was set to 2. Only high-scoring peptides were considered utilizing a false discovery rate (FDR) of <1%, and only one unique high-scoring peptide was required for inclusion of a given identified protein. Factors included in analysis were abundance ratios, *P* values, adjusted *P* values, SEQUEST-HT, PEP scores, percentage coverage, peptide spectral matches, the number of peptides, and unique peptides observed.

Abundance ratio was calculated by pairwise comparisons of experimental/control groups. Pairwise comparisons are shown in Table 1. Results from pairwise comparison of CBA-SHAM versus VEH-SHAM are referred to as CBA-mediated effects, and a full list of significant differentially expressed proteins are listed in Supplemental Table S1 (all Supplemental material is available at https://doi.org/10.6084/m9.figshare.14593653). Results from pairwise comparison of VEH-OVX versus VEH-SHAM are referred to as OVX-mediated effects and a full list of significant differentially expressed proteins are listed in Supplemental Table S2. Results from pairwise comparison of CBA-OVX versus VEH-OVX are referred to as CBA effects in the context of OVX, and a full list of significant differentially expressed proteins are listed in Supplemental Table S3. Results from pairwise comparison of CBA-OVX versus CBA-SHAM are referred to as OVX effects in the context of CBA, and a full list of significant differentially expressed proteins are listed in Supplemental Table S4. The proteomics data have been deposited to the ProteomeXchange Consortium via the PRIDE partner repository (63, 64) with the data set identifier PXD023076 and 10.6019/PXD023076.

Bioinformatic analyses were performed using Qiagen Ingenuity Pathway Analysis (IPA) software (QIAGEN Inc., https://www.qiagenbioinformatics.com/products/ingenuity-pathway-analysis). Proteins with at least a 1.5-fold change (up or down) with a *P* value (FDR) of 0.05 were considered in the core analysis to identify enriched biological processes and the most significant canonical pathways, diseases, and disorders. In an expression analysis, IPA calculates *z*-scores, or activation predictions, for a functional annotation or disease. Unlike the

Table 1. *Pairwise comparisons for omental adipose tissue proteomic data analysis*

Comparison	Result
CBA-SHAM vs. VEH-SHAM	CBA effects
VEH-OVX vs. VEH-SHAM	OVX effects
CBA-OVX vs. VEH-OVX	CBA effects in the context of OVX
CBA-OVX vs. CBA-SHAM	OVX effects in the context of CBA

VEH-SHAM (*n* = 4); CBA-SHAM (*n* = 4); VEH-OVX (*n* = 5); CBA-OVX (*n* = 3). CBA, chronic binge alcohol; OVX, ovariectomy; VEH, vehicle.

P value, the *z*-score takes into account the direction of protein expression. A negative *z*-score indicates a functional activity or pathway that is inhibited, and a positive *z*-score indicates functional activity or pathway activation. Principal component analysis was performed on proteomic data of over 1,429 proteins using scikit-learn version 0.23.1 Python code library.

RESULTS

Body Composition Measurements

No significant differences in percent change in body weight from pre-OVX to study end point, percent change in BMI from pre-OVX to study end point, or change in percent fat from pre-OVX to study end point were observed among the four treatment groups.

CBA and OVX Differentially Alter OmAT Proteomic Profile of SIV-Infected Rhesus Macaques

A total of 1,429 proteins were identified and quantified by proteomic profiling of OmAT samples. A volcano plot of differentially regulated proteins by CBA (1A) and OVX (1B) is shown in Fig. 1. The red circles depict data with significant *P* values ($\leq$0.05) and absolute fold change (FC) value of at least 1.5.

CBA significantly upregulated 14 proteins and downregulated 75 proteins, as shown in the Venn diagram (Fig. 2*A*). CBA in the context of OVX (CBA-OVX vs. VEH-OVX) significantly upregulated 111 proteins and downregulated 25 proteins (Fig. 2*A*). A total of 12 proteins were significantly differentially regulated by CBA (CBA-SHAM vs. VEH-SHAM) and in the context of OVX (CBA-OVX vs. VEH-OVX), which are shown below each Venn diagram. Of these 12 proteins, 4 were significantly upregulated (acetyl-CoA carboxylase alpha, ACACA; ATP citrate lyase, ACLY; fatty acid synthase, FASN; phosphoserine aminotransferase 1, PSAT1) and 8 were significantly downregulated (coiled-coil domain containing 50, CCDC50; histone H1A, H1A; heterogeneous nuclear ribonucleoprotein D, HNRNPD; galectin-3, LGALS3; serum amyloid A protein, SAA1; translocation protein SEC62, SEC62; PKD domain-containing protein, EGK_13856; uncharacterized protein, EGK_04932).

OVX significantly upregulated 47 proteins and downregulated 40 proteins, as shown in the Venn diagram (Fig. 2*B*). OVX in the context of CBA (CBA-OVX vs. CBA-SHAM) significantly upregulated 83 proteins and significantly downregulated 58 proteins of the OmAT proteome (Fig. 2*B*). A total of 14 proteins were significantly differentially regulated by OVX (VEH-OVX vs. VEH-SHAM) and OVX in the context of CBA (CBA-OVX vs. CBA-SHAM). Of these 14 proteins, 9 were significantly upregulated (Acetyl-CoA Carboxylase Beta, ACACB; Alcohol dehydrogenase 1B, ADH1B; Aldehyde Dehydrogenase 1 Family Member L1, ALDH1L1; amine oxidase, AO; FASN; NADH dehydrogenase flavoprotein 1, NDUFV1; peptidyl-prolyl cis-trans isomerase F, PPIF; protein S100, S100; uncharacterized protein, EGK_08523) and 5 were significantly downregulated (asparaginyl endopeptidase, AEP; immunoglobulin heavy chain variable 4, IGHV4; perilipin-4, PLIN4; stabilin-1, STAB1; threonine synthase-like 2, THNSL2). Notably, many of these common proteins, among all 4 comparisons, are involved in pathways related to the OmAT metaboproteome.

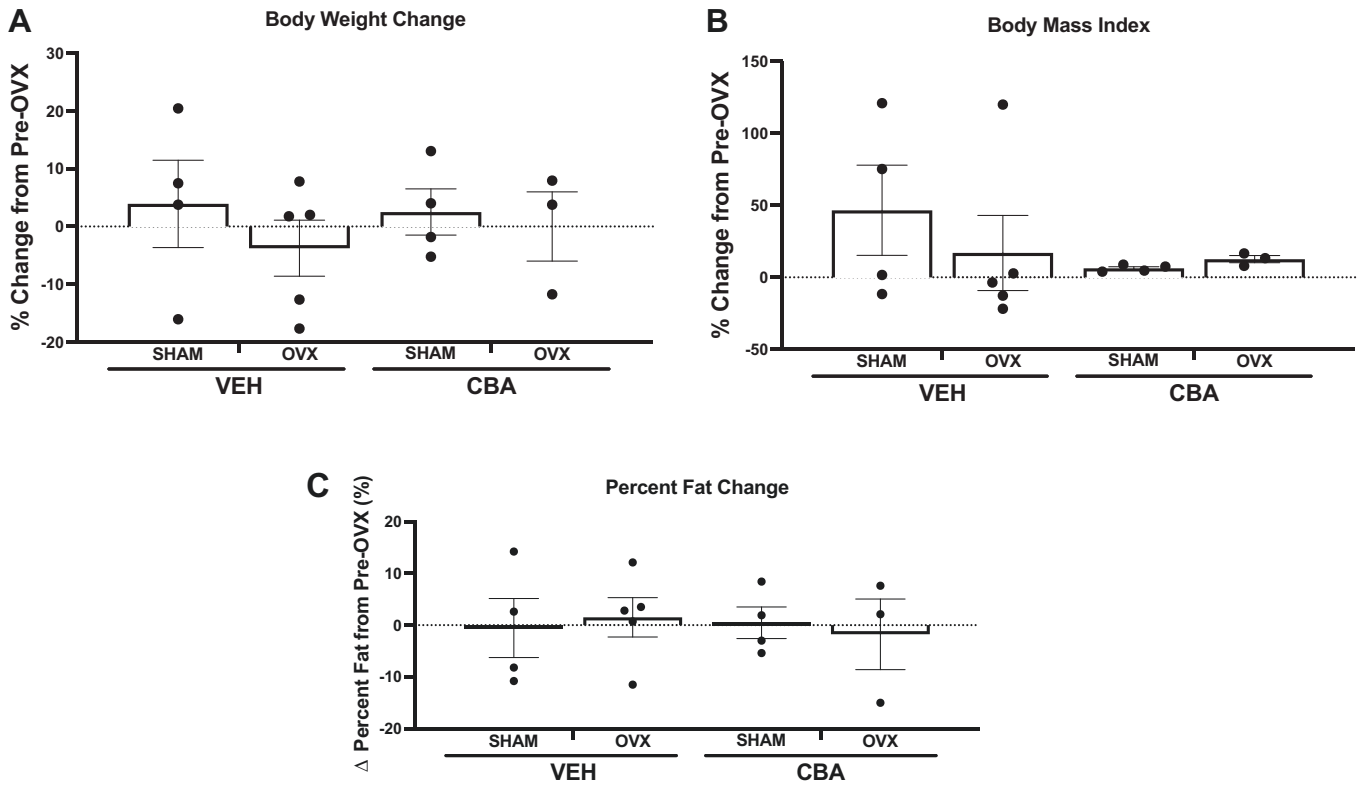

Figure 1. Body weight and body composition measurements. *A*: percent change in body weight from preovariectomy (pre-OVX) to study end point. *B*: percent change in body mass index from pre-OVX to study end point. *C*: change in percent body fat from pre-OVX to study end point. *n* = No. of animals per group; VEH-SHAM (*n* = 4); CBA-SHAM (*n* = 4); VEH-OVX (*n* = 5); CBAOVX (*n* = 3); data analyzed using 2-way ANOVA.

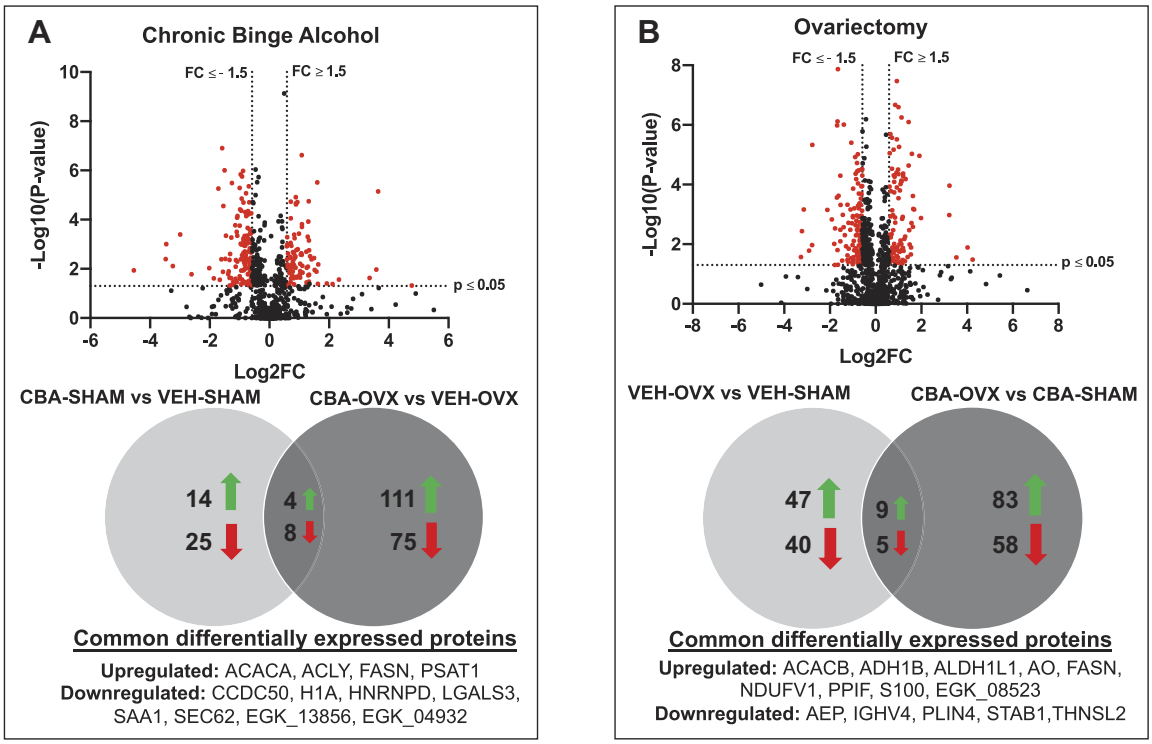

Figure 2. Graphical representation of omental adipose tissue proteomics data based on chronic binge alcohol (CBA; *A*) and ovariectomy (OVX; *B*) effects. *A*: volcano plot of proteomics data based on CBA effects shown as *P* values vs. fold change (FC). CBA upregulated 14 proteins and downregulated 25 proteins in omental adipose tissue. CBA in the context of OVX upregulated 111 proteins and downregulated 75 proteins. CBA in both comparisons upregulated four common proteins and downregulated eight common proteins, listed below the Venn diagram. *B*: volcano plot of proteomics data based on OVX effects shown as *P* values vs. fold change (FC). OVX upregulated 47 proteins and downregulated 40 proteins. OVX in the context of CBA upregulated 83 proteins and downregulated 58 proteins. OVX in both comparisons upregulated nine common proteins and downregulated five common proteins, listed below the Venn diagram. Red points in volcano plot represent data points with $P \leq 0.05$ and a fold change ≥ 1.5. ACACA, acetyl-CoA carboxylase alpha; ACACB, acetyl-CoA carboxylase beta; ACLY, ATP citrate lyase; ADH1B, alcohol dehydrogenase 1B; ALDH1L1, aldehyde dehydrogenase 1 family member L1; AEP, asparaginyl endopeptidase; AO, amine oxidase; CCDC50, coiled-coil domain containing 50; EGK_04932, uncharacterized protein; EGK_08523, uncharacterized protein; EGK_13856, PKD domain-containing protein; FASN, fatty acid synthase; H1A, histone H1A; HNRNPD, heterogeneous nuclear ribonucleoprotein D; IGHV4, immunoglobulin heavy chain variable 4; LGALS3, galectin-3; PLIN4, perilipin-4; PSAT1, phosphoserine aminotransferase 1; NDUFV1, NADH dehydrogenase flavoprotein 1; PPIF, peptidyl-prolyl cis-trans isomerase F; S100, protein S100; SAA1, serum amyloid A protein; SEC62, translocation protein SEC62; STAB1, stabilin-1; THNSL2, threonine synthase-like 2.

To better understand how CBA and OVX affect OmAT proteome, we utilized PCA to compare the proteomic profiles from all four treatment groups. PCA analysis revealed two principal components (PCs) that best accounted for the variability in our data set (Fig. 3). PC1, which accounts for 21.27% of variability, clusters proteomic profiles based on OVX (Fig. 3), whereas PC2, which accounts for 19.24% of variability, clusters proteomic profiles based on CBA (Fig. 3). PC3 explained ~10% of the overall variance within the data (not shown).

Canonical Pathways Affected by CBA

To understand functional mechanisms associated with CBA- and OVX-mediated differentially expressed proteins, the proteomic data set was submitted to IPA core analysis (65). The top-enriched categories of canonical pathways with a *P* value less than 10^{-3} and representative differentially expressed proteins in each canonical pathway are listed in Tables 2 and 3. Notably, there were six canonical pathways affected by both CBA and CBA in the context of OVX. They were "biotin-carboxyl carrier protein assembly," "adenosine monophosphate-activated protein kinase (AMPK) signaling," "liver X receptor/retinoid X receptor (LXR/RXR) activation," "acetyl-CoA biosynthesis III (from citrate)," "peroxisome proliferator-activated receptor alpha/retinoid X receptor alpha (PPARα/RXRα) activation," and "thyroid receptor/retinoid X receptor (TR/RXR) activation" (Table 2).

Canonical Pathways Affected by OVX

There were nine canonical pathways affected by both OVX and OVX in the context of CBA. "liver X receptor/retinoid X receptor (LXR/RXR) activation," "farnesoid X receptor/retinoid X receptor (FXR/RXR) activation," "clathrin-mediated endocytosis signaling," "sirtuin signaling," "acetyl-CoA biosynthesis III (from citrate)," "xenobiotic metabolism aryl hydrocarbon receptor (AHR) signaling pathway," "palmitate biosynthesis I (animals)," "fatty acid biosynthesis initiation II," and "PPARα/RXRα activation" (Table 3).

Directionality of Effects on Pathways Affected by CBA and OVX

IPA core analysis provides *z*-score values indicating predicted pathway activation (positive values) or inhibition (negative values). Figure 4 depicts the top canonical pathways

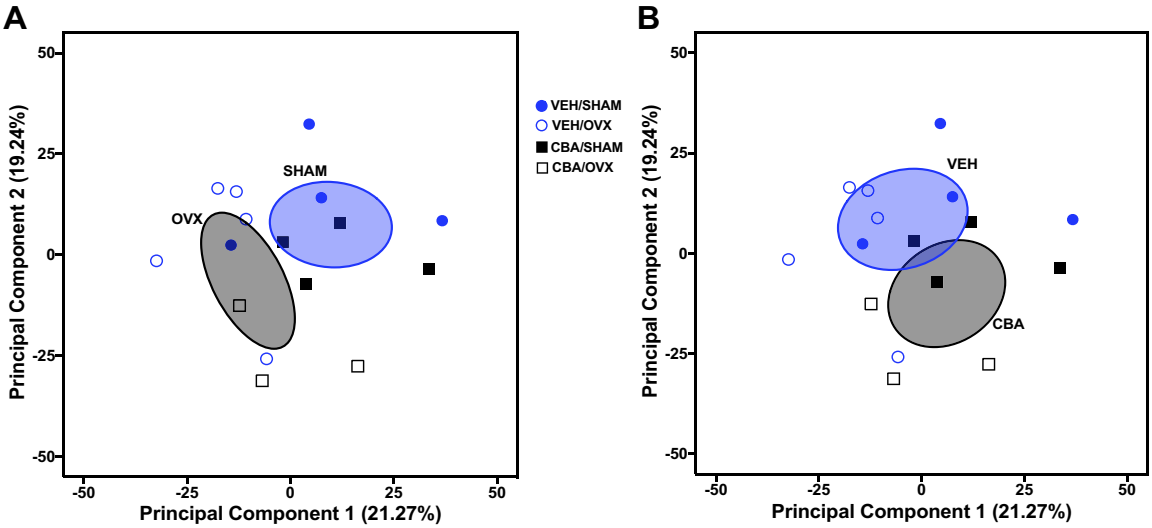

Figure 3. Principal component analysis (PCA) score plot of proteomics data. The PCA plot represents >1,400 proteins that were expressed in all samples/groups. *A*: proteomic profiles of ovariectomy (OVX) and sham surgery animals separate along principal component 1, which explains 21.27% of variability in our data set. *B*: proteomic profiles of chronic binge alcohol (CBA) and vehicle animals separate along principal component 2, which explains 19.24% of variability in our data set. Cluster ellipses are 95% confidence intervals that wrap around the estimated cluster midpoint. VEH-SHAM ($n = 4$); CBA-SHAM ($n = 4$); VEH-OVX ($n = 5$); CBA-OVX ($n = 3$).

with a calculated *z*-score for each comparison. CBA inhibited AMPK signaling pathway (Fig. 4*A*). CBA in the context of OVX inhibited pathways associated with insulin receptor signaling, whereas activating pathways associated with necroptosis, fatty acid β-oxidation, tricarboxylic acid cycle (TCA) cycle, and oxidative phosphorylation (Fig. 4*B*).

OVX inhibited the sirtuin signaling pathway (Fig. 4, *C*–*D*). Most notably, OVX activated PPARα/RXRα activation and LXR/RXR activation pathways, but in the context of CBA, OVX inhibited these same pathways.

Metabolic Disease Pathways Affected by CBA and OVX

In addition to canonical pathways, downstream "diseases and functions" categories were identified for all four comparisons. Analysis of each pairwise comparison revealed "metabolic disease" as a top disease category (Fig. 5). Functional pathways associated with "metabolic disease" were not significantly enriched by CBA. OVX activated five functional pathways associated with "metabolic disease" (Fig. 5*A*), and OVX in the context of CBA activated two functional pathways and inhibited one functional pathway associated with "metabolic disease" (Fig. 5*B*). In contrast, CBA in the context of OVX inhibited five pathways associated with "metabolic disease" (Fig. 5*C*).

Comparison Analysis of Diseases and Biofunctions Affected by CBA and OVX

Examination of the *z*-score-based heat map values for a given pathway, disease, or biofunction revealed differences among the four experimental comparisons (Fig. 6). For example, proteome changes due to CBA or OVX are associated with a strong activation of pathways associated with carbohydrate quantity and lipid concentration, whereas in combination, CBA and OVX did not produce significant changes in these pathways. In addition, CBA in the context of OVX inhibited both apoptosis and necrosis pathways, whereas OVX in the context of CBA led to the activation of apoptosis and necrosis pathways.

DISCUSSION

We examined the effects of CBA and OVX on the OmAT proteome in SIV-infected macaques. Our quantitative discovery-based proteomic approach identified commonalities and differences in OmAT protein expression profiles due to CBA, OVX, and their combination. Our results identified functional pathways associated with protein changes centered around the "OmAT metaboproteome profile." Specifically, our results show predominant OVX-mediated OmAT metaboproteome dysregulation with most significant number of differentially regulated proteins and their implicated pathways. CBA appears to be an effect modifier of the OVX-associated changes.

CBA-Mediated Effects in SIV-Infected Macaques

The negative effects of chronic alcohol on adipose tissue biology and metabolic function have been extensively investigated (22, 23, 25, 66–69). In a male macaque SIV model, we have previously published that CBA accelerates SIV-disease progression and promotes whole body and adipose tissue-specific metabolic dysfunction including changes in insulin-glucose dynamics and changes in adipose tissue collagen content, inflammatory cell infiltration, and adiponectin secretion (10, 13, 44, 45, 70). However, in our current study, IPA analyses revealed that CBA administration did not produce large-scale differential regulation of canonical pathways or functional pathways of metabolic disease. CBA administration induced protein changes that promote inhibition of the AMPK signaling pathway. In support of previous findings showing alcohol-induced increases in cell death (68, 71), CBA administration increased protein expression associated with activation of both apoptosis and necrosis pathways. Despite several studies reporting evidence for

Table 2. *Canonical pathways affected by CBA and CBA in the context of OVX*

Ingenuity Canonical Pathway	*P* Value of Overlap	Ratio
CBA effects		
Biotin-carboxyl carrier protein assembly*	8.15E-06	2/3
AMPK signaling*	4.38E-04	4/214
LXR/RXR activation*	1.08E-03	3/121
Acetyl-CoA biosynthesis III (from citrate)*	1.67E-03	1/1
Myc-mediated apoptosis signaling	3.17E-03	2/50
Palmitate biosynthesis I (animals)	3.34E-03	1/2
Fatty acid biosynthesis initiation II	3.34E-03	1/2
PPARα/RXRα activation*	3.91E-03	3/190
RAR activation	4.14E-03	3/194
TR/RXR activation*	8.70E-03	2/84
BMP signaling pathway	8.90E-03	2/85
CBA in the context of OVX		
Mitochondrial dysfunction	1.80E-21	22/171
Oxidative phosphorylation	7.73E-17	16/109
Acute phase response signaling	8.21E-16	18/179
TCA cycle II (eukaryotic)	4.77E-14	9/24
Sirtuin signaling pathway	3.73E-11	17/291
Isoleucine degradation I	9.34E-10	6/16
LXR/RXR activation*	1.18E-09	11/121
FXR/RXR activation	1.83E-09	11/26
Glutaryl-CoA degradation	7.30E-08	5/16
Acetyl-CoA biosynthesis I (pyruvate dehydrogenase complex)	8.76E-08	4/7
Fatty acid β-oxidation I	9.61E-08	6/32
Coagulation system	1.69E-07	6/35
Valine degradation I	1.91E-07	5/19
Ketolysis	5.17E-07	4/10
Tryptophan degradation III (eukaryotic)	5.40E-07	5/23
Ketogenesis	8.08E-07	4/11
Mevalonate pathway I	2.41E-06	4/14
2-ketoglutarate dehydrogenase complex	3.58E-06	3/5
Extrinsic prothrombin activation pathway	4.33E-06	4/16
Superpathway of geranylgeranyldiphosphate biosynthesis I (via mevalonate)	7.20E-06	4/18
Intrinsic prothrombin activation pathway	1.22E-05	5/42
Superpathway of cholesterol biosynthesis	5.26E-05	4/29
Biotin-carboxyl carrier protein assembly*	1.53E-04	2/3
Neuroprotective role of THOP1 in Alzheimer's disease	1.92E-04	6/116
GP6 signaling pathway	2.20E-04	6/119
Branched-chain α-keto acid dehydrogenase complex	3.04E-04	2/4
Hepatic fibrosis signaling pathway	3.36E-04	10/368
TR/RXR activation*	3.48E-04	5.84
Stearate biosynthesis I (animals)	3.87E-04	4/48
2-Oxobutanoate degradation I	5.04E-04	2/5
Folate polyglutamylation	5.04E-04	2/5
Tight junction signaling	1.36E-03	6/168
Ethanol degradation II	1.54E-03	3/32
Role of tissue factor in cancer	1.56E-03	5/117
Folate transformations I	1.78E-03	2/9
Noradrenaline and adrenaline degradation	2.00E-03	3/35
Glycine betaine degradation	2.21E-03	2/10
superpathway of methionine degradation	2.35E-03	3/37
Complement system	2.35E-03	3/37
PPARα/RXRα activation*	2.53E-03	6/190
Estrogen receptor signaling	2.59E-03	8/328
Iron homeostasis signaling pathway	3.11E-03	5/137
Calcium signaling	3.77E-03	6/206
AMPK signaling*	4.53E-03	6/214
Epithelial adherens junction signaling	4.84E-03	5/152
γ-linolenate biosynthesis II (animals)	6.47E-03	2/17
Methylthiopropionate biosynthesis	7.17E-03	1/1
Acetyl-CoA biosynthesis III (from citrate)*	7.17E-03	1/1
Sorbitol degradation I	7.17E-03	1/1

Ratio is the number of differentially expressed proteins in our data set that were implicated in the pathway relative to the total number of proteins in that pathway. AMPK, adenosine monophosphate-activated protein kinase; CBA, chronic binge alcohol; FXR, farnesoid X receptor; LXR, liver X receptor; OVX, ovariectomy; PPARα, peroxisome proliferator-activated receptor alpha; RXR, retinoid X receptor. Only pathways with *P* value of overlap 10^{-3} are shown. *Pathways that are enriched in both comparisons.

Table 3. *Canonical pathways affected by OVX and OVX in the context of CBA*

Ingenuity Canonical Pathway	*P* Value of Overlap	Ratio
OVX effects		
Acute phase response signaling	6.57E-13	13/179
LXR/RXR activation*	2.23E-09	9/121
FXR/RXR activation*	3.19E-09	9/126
Clathrin-mediated endocytosis signaling*	1.30E-07	9/193
Coagulation system	3.55E-07	5/35
Atherosclerosis signaling	1.66E-05	6/127
Neuroprotective role of THOP1 in Alzheimer's disease	1.34E-04	5/116
Production of nitric oxide and reactive oxygen species in macrophages	1.48E-04	6/188
IL-12 signaling and production in macrophages	2.45E-04	5/132
Intrinsic prothrombin activation pathway	7.43E-04	3/42
Sirtuin signaling pathway*	1.48E-03	6/291
Extrinsic prothrombin activation pathway	2.04E-03	2/16
Caveolar-mediated endocytosis signaling	3.66E-03	3/73
Macropinocytosis signaling	4.10E-03	3/76
Acetyl-CoA biosynthesis III (from Citrate)*	4.22E-03	1/1
Apelin liver signaling pathway	5.37E-03	2/26
Xenobiotic metabolism AHR signaling pathway*	5.61E-03	3/85
Palmitate biosynthesis I (animals)*	8.43E-03	1/2
Fatty acid biosynthesis Initiation II*	8.43E-03	1/2
PPARα/RXRα activation*	8.64E-03	4/190
Xenobiotic metabolism PXR signaling pathway	8.95E-03	4/192
OVX in the context of CBA		
Mitochondrial dysfunction	1.05E-12	13/171
Oxidative phosphorylation	7.55E-11	10/109
Sirtuin signaling pathway*	8.18E-10	13/291
Glutaryl-CoA degradation	7.21E-07	4/16
Valine degradation I	1.52E-06	4/19
Tryptophan degradation III (eukaryotic)	3.42E-06	4/23
Ketolysis	1.09E-05	3/10
Fatty acid β-oxidation I	1.35E-05	4/32
Ketogenesis	1.49E-05	3/11
LXR/RXR activation*	1.99E-05	6/121
Mevalonate pathway I	3.26E-05	3/14
Isoleucine degradation I	4.99E-05	3/16
Biotin-carboxyl carrier protein assembly	6.20E-05	2/3
Stearate biosynthesis I (animals)	6.88E-05	4/48
Superpathway of geranylgeranyldiphosphate biosynthesis I (via mevalonate)	7.22E-05	3/18
TCA cycle II (eukaryotic)	1.75E-04	3/24
NRF2-mediated oxidative stress response	2.35E-04	6/189
Superpathway of cholesterol biosynthesis	3.12E-04	3/29
Ethanol degradation II	4.19E-04	3/32
Iron homeostasis signaling pathway	4.21E-04	5/137
Acetyl-CoA biosynthesis I (pyruvate dehydrogenase complex)	4.29E-04	2/7
AMPK signaling	4.57E-04	6/214
Noradrenaline and adrenaline degradation	5.47E-04	3/35
Superoxide radicals degradation	5.70E-04	2/8
Xenobiotic metabolism AHR signaling pathway*	6.29E-04	4/85
Sucrose degradation V (mammalian)	7.31E-04	2/9
Folate transformations I	7.31E-04	2/9
Glycine betaine degradation	9.10E-04	2/10
Acyl-CoA hydrolysis	1.56E-03	2/13
PPARα/RXRα activation*	1.82E-03	5/190
Clathrin-mediated endocytosis signaling*	1.95E-03	5/193
FXR/RXR activation*	2.70E-03	4/126
Serotonin degradation	3.60E-03	3/67
LPS/IL-1 mediated inhibition of RXR function	3.71E-03	5/224
Aryl hydrocarbon receptor signaling	4.24E-03	4/143
Acetyl-CoA biosynthesis III (from citrate)*	4.57E-03	1/1
Glycolysis I	6.27E-03	2/26
Gluconeogenesis I	6.27E-03	2/26
Palmitate biosynthesis I (animals)*	9.13E-03	1/2
Fatty acid biosynthesis initiation II*	9.13E-03	1/2
Glycine biosynthesis I	9.13E-03	1/2

Ratio is the number of differentially expressed proteins in our data set that were implicated in the pathway relative to the total number of proteins in that pathway. AHR, aryl hydrocarbon receptor; AMPK, adenosine monophosphate-activated protein kinase; CBA, chronic binge alcohol; FXR, farnesoid X receptor; LXR, liver X receptor; OVX, ovariectomy; PPARα, peroxisome proliferator-activated receptor alpha; RXR, retinoid X receptor. Only pathways with *P* value of overlap 10^{-3} are shown. *Pathways that are enriched in both comparisons.

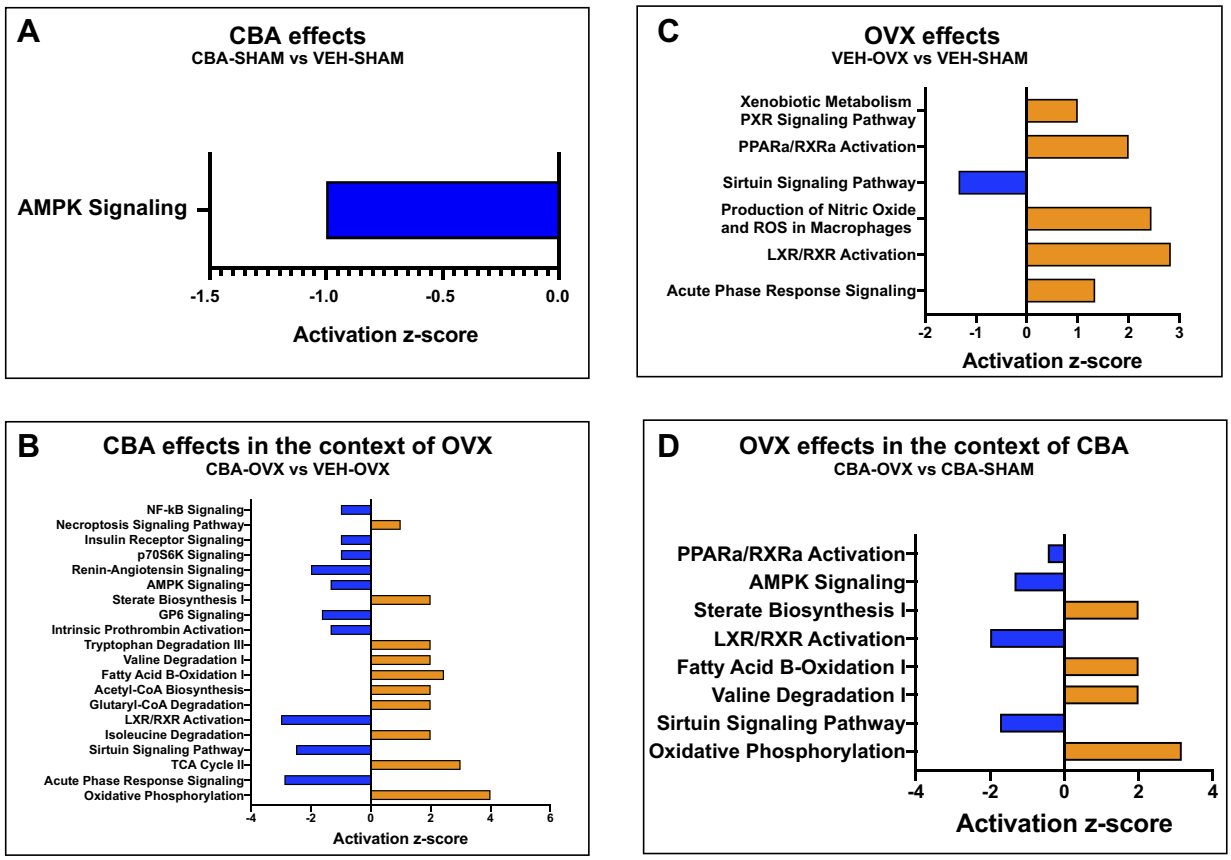

Figure 4. Canonical pathways associated with protein changes between chronic binge alcohol (CBA) and ovariectomy (OVX) groups with calculated *z*-scores, whereas a negative *z*-score indicates inhibition of the pathway, and a positive *z*-score indicates pathway activation. *A*: canonical pathway affected by CBA. *B*: a total of 20 canonical pathways were affected by CBA in the context of OVX: 10 inhibited pathways and 10 activated pathways. *C*: a total of six canonical pathways were affected by OVX: one inhibited pathway and five activated pathways. *D*: a total of eight canonical pathways were affected by OVX in the context of CBA: four inhibited pathways and four activated pathways. VEH-SHAM ($n = 4$); CBA-SHAM ($n = 4$); VEH-OVX ($n = 5$); CBA-OVX ($n = 3$).

increased ROS with chronic alcohol exposure, including previous studies from our laboratory in end-stage SIV-infected male macaques, the ROS functional pathway was not significantly altered in the OmAT of female SIV-infected macaques (52, 72–74). These results underscore the importance of further investigation of the effects of CBA on adipose tissue in SIV, as well as the possible sexual dimorphic responses to CBA, to understand the cellular and molecular mechanisms that mediate these differential responses.

In the context of OVX, CBA administration led to much more profound effects on OmAT metaboproteome profile. In agreement with current knowledge of CBA effects on adipose

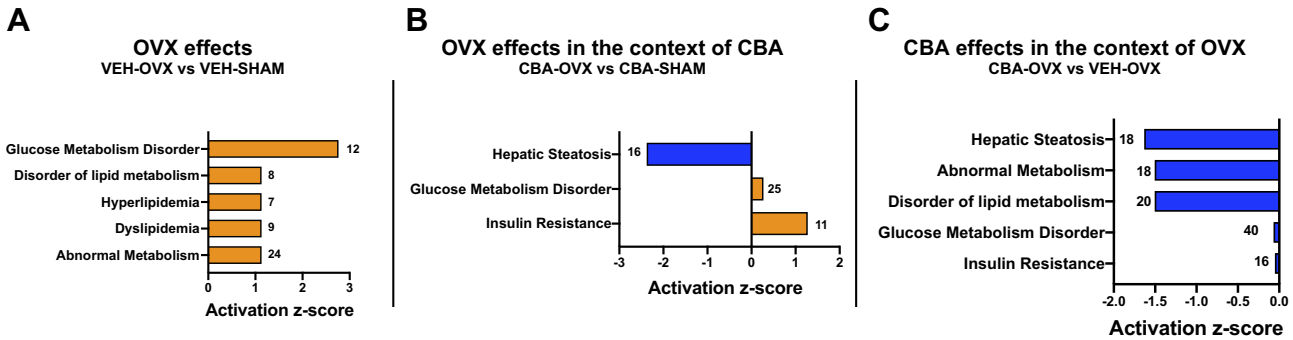

Figure 5. Functional pathways of "metabolic disease" with calculated *z*-scores, wherein a negative *z*-score indicates inhibition of the pathway, and a positive *z*-score indicates pathway activation. *A*: functional pathways of "metabolic disease" predicted to be activated by ovariectomy (OVX). *B*: functional pathways of "metabolic disease" predicted to be inhibited/activated by OVX in the context of chronic binge alcohol (CBA). *C*: functional pathways of "metabolic disease" predicted to be inhibited by CBA in the context of OVX. The number at the end of each bar represents the number of proteins within the pathway that are changed. VEH-SHAM ($n = 4$); CBA-SHAM ($n = 4$); VEH-OVX ($n = 5$); CBA-OVX ($n = 3$).

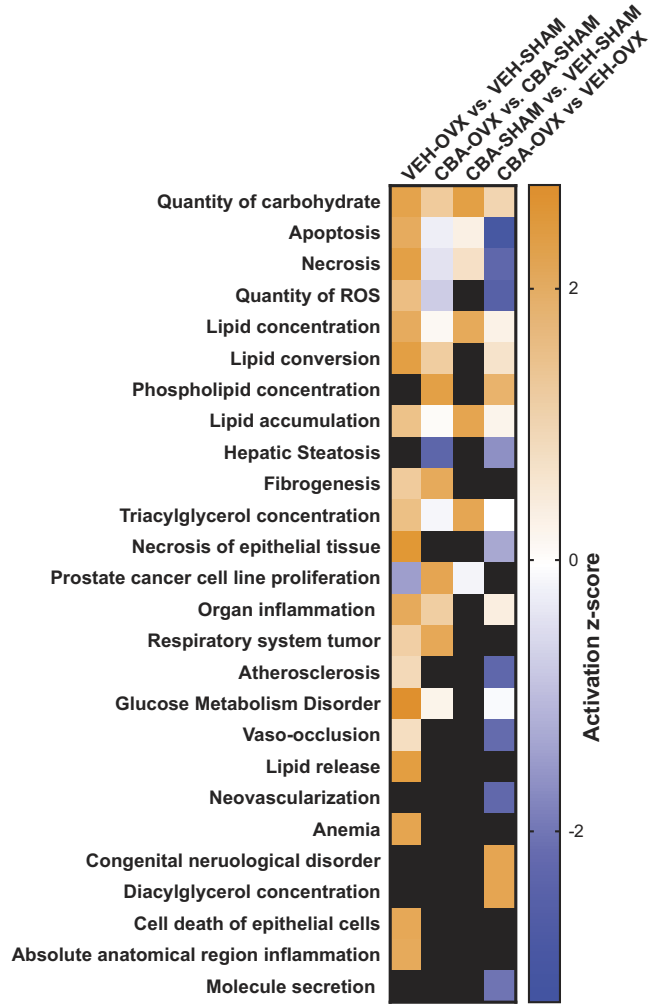

Figure 6. Comparison analysis heat map of top diseases and biofunctions associated with significantly differentially expressed proteins affected by chronic binge alcohol (CBA) and/or ovariectomy (OVX). Square color indicates predicted activation (orange) or inhibition (blue) by Ingenuity Pathway Analysis (IPA). Black squares indicate that disease or biofunction is unaffected. VEH-SHAM ($n = 4$); CBA-SHAM ($n = 4$); VEH-OVX ($n = 5$); CBA-OVX ($n = 3$).

tissue metabolism, pathway analysis revealed that CBA in the context of OVX inhibited insulin receptor signaling and AMPK signaling functional pathways, whereas activating fatty acid oxidation, acetyl-CoA biosynthesis, and glutaryl-CoA degradation pathways. CBA in the context of OVX led to the activation of the TCA cycle and oxidative phosphorylation pathways. These results suggest that ovarian hormone loss potentially plays a more important role than CBA in modulating these pathways. Further investigation is warranted to uncover possible competing mechanisms responsible for these contrasting effects. CBA in the context of OVX led to general inhibition of metabolic disease functional pathways. Specifically, functional pathways of hepatic steatosis, abnormal metabolism, insulin resistance, and disorders of lipid and glucose metabolism were inhibited due to CBA in the context of OVX. These results are in line with reports suggesting that ovariectomized rats were protected from early alcohol-induced organ injury (75). Mechanisms leading to this apparent OVX-mediated "protection" are still unknown and should be further investigated. Whether chronicity or quantity of alcohol use modify these effects remains to be examined.

OVX-Mediated Effects in SIV-Infected Macaques

Our OmAT proteomic results agree with clinically occurring metabolic phenomenon associated with loss of estrogen in women (37, 76–78). The pathway analyses indicated that OVX significantly altered expression of proteins involved in lipid and glucose metabolism. In terms of functional pathways of metabolic disease, OVX differentially regulated proteins that promoted development of glucose and lipid metabolism disorders including hyperlipidemia and dyslipidemia. Risk for metabolic comorbidities increases with menopause, and the transition to postmenopause is associated with occurrence of metabolic dysregulation including lipid, glucose, and insulin dyshomeostasis (76, 78). HIV infection itself and ART also promote the emergence of metabolic comorbidities (2, 34, 79, 80). It is well known that estrogen has important modulatory effects on adipose tissue lipid metabolism (43, 81). It is not completely clear whether menopause in HIV-infected women exacerbates risks for metabolic complications. However, our results in female SIV-infected macaques and the results of comparative studies on risk assessment in uninfected and HIV-infected women suggest that the loss of

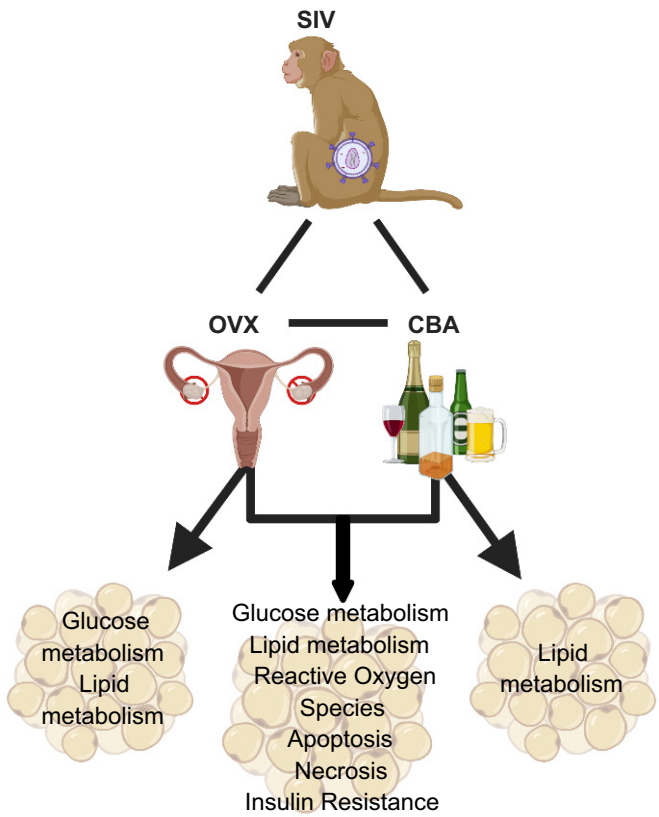

Figure 7. Schematic summary of biofunctions involved in alcohol- and ovariectomy-mediated adipose tissue metaboproteome dysregulation in simian immunodeficiency virus (SIV) disease. CBA, chronic binge alcohol; OVX, ovariectomy. [Created with BioRender.com and published with permission.]

estrogen in SIV/HIV further contributes to development of metabolic dysfunction (77, 82).

In addition to major effects on adipose tissue metabolism, OVX also significantly affected cell survival and ROS generation pathways. Specifically, in the OVX groups, differential regulation of proteins indicated activation of apoptosis, necrosis, and ROS in OmAT of SIV-infected macaques. Literature on the effects of estrogen on cell survival is inconsistent. Several studies report that estrogen stimulates growth and inhibits apoptosis through estrogen receptor-mediated mechanisms in many cell types (83–86). On the other hand, there is also strong evidence suggesting that estrogen stimulates apoptosis in other cell types, including breast cancer (83, 85, 87). Our results suggest that estrogen loss in SIV may promote cell death by the activation of apoptosis and necrosis pathways. Whether CBA or OVX increases apoptotic cell death in OmAT is the focus of our ongoing studies.

In the context of CBA, OVX altered protein expression indicating activation of functional pathways associated with metabolic disease including glucose metabolism disorders and insulin resistance. OVX in the context of CBA led to decreased protein expression associated with hepatic steatosis functional pathway. There was strong activation of cell death pathways, specifically apoptosis and necrosis, with OVX in the VEH-OVX versus VEH-SHAM comparison, which contrasts with inhibition of these pathways in the context of CBA. Whether CBA results in a functional attenuation of OVX-mediated cell death and ROS will be pursued in ongoing studies.

This investigation was not without limitations. One limitation is the small sample size, and global proteomic analysis was performed on a subset of OmAT samples which is part of a larger parent study. Ongoing work will include protein validation and identify the functional relevance in the full set of OmAT samples obtained from the parent study. Another limitation is the use of only one complete package software, Proteome Discoverer (PD), for both identification and quantification of proteomic data sets. However, PD is a very powerful software tool for identification of peptides and proteins. PD has been previously used in several published manuscripts from LSUHSC's Proteomics Core Facility (58–60).

Together, these results provide evidence for the role of ovarian hormone loss (estrogen being the major hormone) in mediating OmAT metaboproteome dysregulation in SIV and suggest that chronic alcohol exposure is an effect modifier in the context of OVX (Fig. 7). Our findings indicate that in the comparison between CBA-SHAM versus VEH-SHAM, CBA does not dysregulate many proteins of pathways associated with metabolic disease. However, OVX promotes pathways associated with the development of metabolic disease. The data also suggest that CBA administration in the context of OVX produced larger metabolic and cellular effects, suggesting a possible protective role of estrogen against CBA-mediated adipose tissue injury in female SIV-infected macaques. Further investigation is necessary to determine whether and how this protection is mediated in OmAT. Ongoing studies will investigate the functional significance of alcohol and OVX-mediated OmAT metaboproteome derangements on adipocyte metabolic capacity. The implications of alcohol use and OVX on omental adipose tissue metaboproteome resulting in alterations in glucose and lipid metabolism and metabolic disease pathways in this study may help formulate recommendations to reduce risk of metabolic comorbidities among HIV-infected women.

SUPPLEMENTAL DATA

Supplemental Tables S1–S4: https://doi.org/10.6084/m9.figshare.14593653.

ACKNOWLEDGMENTS

The authors acknowledge Ronald G. Budnar Jr. and Dr. Vince Maffei for performing Principal Component Analysis of the proteomic data. The authors acknowledge Dr. Jeffrey Schumacher and Dr. Jason Dufour, Tulane National Research Primate Center, for veterinary expertise. From LSUHSC-NO, we are grateful for the technical and veterinary support of Larry Coleman, Heather McGarrah, and Amy Weinberg. We also are grateful for the technical expertise of Nedra Lacour, Bryant Autin, Jasmine Hall, Curtis Vande Stouwe, Jane Schexnayder, and Rhonda Martinez.

GRANTS

The research was supported by National Institute on Alcohol Abuse and Alcoholism Grants 5P60AA009803-25, 5T32AA007577-20, and 1F31AA028459-01.

DISCLOSURES

No conflicts of interest, financial or otherwise, are declared by the authors.

AUTHOR CONTRIBUTIONS

J.M.P., L.S., and P.E.M. conceived and designed research; J.M.P. and J.J.G. performed experiments; J.M.P. analyzed data; J.M.P. interpreted results of experiments; J.M.P. prepared figures; J.M.P. drafted manuscript; J.M.P., J.J.G., L.S., and P.E.M. edited and revised manuscript; J.M.P., J.J.G., L.S., and P.E.M. approved final version of manuscript.

REFERENCES

1. **Centers for Disease Control and Prevention**. Estimated HIV incidence and prevalence in the United States, 2014–2018 (Online). http://www.cdc.gov/hiv/library/reports/hiv-surveillance.html.
2. **Paula AA**, **Falcão MC**, **Pacheco AG.** Metabolic syndrome in HIV-infected individuals: underlying mechanisms and epidemiological aspects. *AIDS Res Ther* 10: 32, 2013. doi:10.1186/1742-6405-10-32.
3. **Willig AL**, **Overton ET.** Metabolic consequences of HIV: pathogenic insights. *Curr HIV/AIDS Rep* 11: 35–44, 2014. doi:10.1007/s11904-013-0191-7.
4. **de Pommerol M**, **Hessamfar M**, **Lawson-Ayayi S**, **Neau D**, **Geffard S**, **Farbos S**, **Uwamaliya B**, **Vandenhende MA**, **Pellegrin JL**, **Blancpain S**, **Dabis F**, **Morlat P**; **Groupe d'Epidémiologie Clinique du SIDA en Aquitaine (GECSA).** Menopause and HIV infection: age at onset and associated factors, ANRS CO3 Aquitaine cohort. *Int J STD AIDS* 22: 67–72, 2011. doi:10.1258/ijsa.2010.010187.
5. **Fantry LE**, **Zhan M**, **Taylor GH**, **Sill AM**, **Flaws JA.** Age of menopause and menopausal symptoms in HIV-infected women. *AIDS Patient Care STDS* 19: 703–711, 2005. doi:10.1089/apc.2005.19.703.
6. **Crane HM**, **McCaul ME**, **Chander G**, **Hutton H**, **Nance RM**, **Delaney JAC**, **Merrill JO**, **Lau B**, **Mayer KH**, **Mugavero MJ**, **Mimiaga M**, **Willig JH**, **Burkholder GA**, **Drozd DR**, **Fredericksen RJ**, **Cropsey K**, **Moore RD**, **Simoni JM**, **Christopher Mathews W**, **Eron JJ**, **Napravnik S**, **Christopoulos K**, **Geng E**, **Saag MS**, **Kitahata MM.** Prevalence and factors associated with hazardous alcohol use among persons living with HIV across the US in the current era of antiretroviral treatment. *AIDS Behav* 21: 1914–1925, 2017. doi:10.1007/s10461-017-1740-7.

7. **Galvan FH**, **Bing EG**, **Fleishman JA**, **London AS**, **Caetano R**, **Burnam MA**, **Longshore D**, **Morton SC**, **Orlando M**, **Shapiro M.** The prevalence of alcohol consumption and heavy drinking among people with HIV in the United States: results from the HIV Cost and Services Utilization Study. *J Stud Alcohol* 63: 179–186, 2002. doi:10.15288/jsa.2002.63.179.
8. **Samet JH**, **Phillips SJ**, **Horton NJ**, **Traphagen ET**, **Freedberg KA.** Detecting alcohol problems in HIV-infected patients: use of the CAGE questionnaire. *AIDS Res Hum Retroviruses* 20: 151–155, 2004. doi:10.1089/088922204773004860.
9. **Baum MK**, **Rafie C**, **Lai S**, **Sales S**, **Page JB**, **Campa A.** Alcohol use accelerates HIV disease progression. *AIDS Res Hum Retroviruses* 26: 511–518, 2010. doi:10.1089/aid.2009.0211.
10. **Amedee AM**, **Nichols WA**, **Robichaux S**, **Bagby GJ**, **Nelson S.** Chronic alcohol abuse and HIV disease progression: studies with the non-human primate model. *Curr HIV Res* 12: 243–253, 2014. doi:10.2174/1570162x12666140721115717.
11. **Cheng DM**, **Libman H**, **Bridden C**, **Saitz R**, **Samet JH.** Alcohol consumption and lipodystrophy in HIV-infected adults with alcohol problems. *Alcohol* 43: 65–71, 2009. doi:10.1016/j.alcohol.2008.09.004.
12. **Marshall BDL**, **Tate JP**, **McGinnis KA**, **Bryant KJ**, **Cook RL**, **Edelman EJ**, **Gaither JR**, **Kahler CW**, **Operario D**, **Fiellin DA**, **Justice AC.** Long-term alcohol use patterns and HIV disease severity. *AIDS* 31: 1313–1321, 2017. doi:10.1097/QAD.0000000000001473.
13. **Molina PE**, **McNurlan M**, **Rathmacher J**, **Lang CH**, **Zambell KL**, **Purcell J**, **Bohm RP**, **Zhang P**, **Bagby GJ**, **Nelson S.** Chronic alcohol accentuates nutritional, metabolic, and immune alterations during asymptomatic simian immunodeficiency virus infection. *Alcohol Clin Exp Res* 30: 2065–2078, 2006. doi:10.1111/j.1530-0277.2006.00252.x.
14. **Molina PE**, **Simon L**, **Amedee AM**, **Welsh DA**, **Ferguson TF.** Impact of alcohol on HIV disease pathogenesis, comorbidities and aging: integrating preclinical and clinical findings. *Alcohol Alcohol* 53: 439–447, 2018 [Erratum in *Alcohol Alcohol* 53: 636, 2018]. doi:10.1093/alcalc/agy016.
15. **Simon L**, **Ferguson TF**, **Vande Stouwe C**, **Brashear MM**, **Primeaux SD**, **Theall KP**, **Welsh DA**, **Molina PE.** Prevalence of insulin resistance in adults living with HIV: implications of alcohol use. *AIDS Res Hum Retroviruses* 36: 742–752, 2020. doi:10.1089/AID.2020.0029.
16. **Castro AC**, **Silveira EA**, **Falco MO**, **Nery MW**, **Turchi MD.** Overweight and abdominal obesity in adults living with HIV/AIDS. *Rev Assoc Med Bras (1992)* 62: 353–360, 2016. doi:10.1590/1806-9282.62.04.353.
17. **Godfrey C**, **Bremer A**, **Alba D**, **Apovian C**, **Koethe JR**, **Koliwad S**, **Lewis D**, **Lo J**, **McComsey GA**, **Eckard A**, **Srinivasa S**, **Trevillyan J**, **Palmer C**, **Grinspoon S.** Obesity and fat metabolism in human immunodeficiency virus-infected individuals: immunopathogenic mechanisms and clinical implications. *J Infect Dis* 220: 420–431, 2019. doi:10.1093/infdis/jiz118.
18. **Koethe JR**, **Lagathu C**, **Lake JE**, **Domingo P**, **Calmy A**, **Falutz J**, **Brown TT**, **Capeau J.** HIV and antiretroviral therapy-related fat alterations. *Nat Rev Dis Primers* 6: 48, 2020 [Erratum in *Nat Rev Dis Primers* 6: 54, 2020]. doi:10.1038/s41572-020-0181-1.
19. **Lake JE.** The fat of the matter: obesity and visceral adiposity in treated HIV infection. *Curr HIV/AIDS Rep* 14: 211–219, 2017. doi:10.1007/s11904-017-0368-6.
20. **McComsey GA**, **Kitch D**, **Sax PE**, **Tebas P**, **Tierney C**, **Jahed NC**, **Myers L**, **Melbourne K**, **Ha B**, **Daar ES.** Peripheral and central fat changes in subjects randomized to abacavir-lamivudine or tenofovir-emtricitabine with atazanavir-ritonavir or efavirenz: ACTG Study A5224s. *Clin Infect Dis* 53: 185–196, 2011. doi:10.1093/cid/cir324.
21. **Kang L**, **Nagy LE.** Chronic ethanol feeding suppresses beta-adrenergic receptor-stimulated lipolysis in adipocytes isolated from epididymal fat. *Endocrinology* 147: 4330–4338, 2006. doi:10.1210/en.2006-0120.
22. **Kang L**, **Chen X**, **Sebastian BM**, **Pratt BT**, **Bederman IR**, **Alexander JC**, **Previs SF**, **Nagy LE.** Chronic ethanol and triglyceride turnover in white adipose tissue in rats: inhibition of the anti-lipolytic action of insulin after chronic ethanol contributes to increased triglyceride degradation. *J Biol Chem* 282: 28465–28473, 2007. doi:10.1074/jbc.M705503200.
23. **Steiner JL**, **Lang CH.** Alcohol, adipose tissue and lipid dysregulation. *Biomolecules* 7: 16, 2017. doi:10.3390/biom7010016.
24. **Chen X**, **Sebastian BM**, **Nagy LE.** Chronic ethanol feeding to rats decreases adiponectin secretion by subcutaneous adipocytes. *Am J Physiol Endocrinol Metab* 292: E621–E628, 2007. doi:10.1152/ajpendo.00387.2006.
25. **Kang L**, **Sebastian BM**, **Pritchard MT**, **Pratt BT**, **Previs SF**, **Nagy LE.** Chronic ethanol-induced insulin resistance is associated with macrophage infiltration into adipose tissue and altered expression of adipocytokines. *Alcohol Clin Exp Res* 31: 1581–1588, 2007. doi:10.1111/j.1530-0277.2007.00452.x.
26. **Fan AZ**, **Russell M**, **Naimi T**, **Li Y**, **Liao Y**, **Jiles R**, **Mokdad AH.** Patterns of alcohol consumption and the metabolic syndrome. *J Clin Endocrinol Metab* 93: 3833–3838, 2008. doi:10.1210/jc.2007-2788.
27. **Lindtner C**, **Scherer T**, **Zielinski E**, **Filatova N**, **Fasshauer M**, **Tonks NK**, **Puchowicz M**, **Buettner C.** Binge drinking induces whole-body insulin resistance by impairing hypothalamic insulin action. *Sci Transl Med* 5: 170ra14, 2013. doi:10.1126/scitranslmed.3005123.
28. **Oh JE.** Relationship between heavy drinking, binge drinking, and metabolic syndrome in obese and non-obese Korean male adults. *Nutr Res Pract* 12: 166–172, 2018. doi:10.4162/nrp.2018.12.2.166.
29. **Caron M**, **Vigouroux C**, **Bastard JP**, **Capeau J.** Antiretroviral-related adipocyte dysfunction and lipodystrophy in HIV-infected patients: alteration of the PPARγ-dependent pathways. *PPAR Res* 2009: 507141, 2009. doi:10.1155/2009/507141.
30. **Caron M**, **Auclair M**, **Lagathu C**, **Lombès A**, **Walker UA**, **Kornprobst M**, **Capeau J.** The HIV-1 nucleoside reverse transcriptase inhibitors stavudine and zidovudine alter adipocyte functions in vitro. *AIDS* 18: 2127–2136, 2004. doi:10.1097/00002030-200411050-00004.
31. **Gorwood J**, **Bourgeois C**, **Mantecon M**, **Atlan M**, **Pourcher V**, **Pourcher G**, **Le Grand R**, **Desjardins D**, **Fève B**, **Lambotte O**, **Capeau J**, **Béréziat V**, **Lagathu C.** Impact of HIV/simian immunodeficiency virus infection and viral proteins on adipose tissue fibrosis and adipogenesis. *AIDS* 33: 953–964, 2019. doi:10.1097/QAD.0000000000002168.
32. **Lagathu C**, **Bastard JP**, **Auclair M**, **Maachi M**, **Kornprobst M**, **Capeau J**, **Caron M.** Antiretroviral drugs with adverse effects on adipocyte lipid metabolism and survival alter the expression and secretion of proinflammatory cytokines and adiponectin in vitro. *Antivir Ther* 9: 911–920, 2004.
33. **Shikuma CM**, **Gangcuangco LM**, **Killebrew DA**, **Libutti DE**, **Chow DC**, **Nakamoto BK**, **Liang CY**, **Milne CI**, **Ndhlovu LC**, **Barbour JD**, **Shiramizu BT**, **Gerschenson M.** The role of HIV and monocytes/macrophages in adipose tissue biology. *J Acquir Immune Defic Syndr* 65: 151–159, 2014. doi:10.1097/01.qai.0000435599.27727.6c.
34. **Lagathu C**, **Béréziat V**, **Gorwood J**, **Fellahi S**, **Bastard JP**, **Vigouroux C**, **Boccara F**, **Capeau J.** Metabolic complications affecting adipose tissue, lipid and glucose metabolism associated with HIV antiretroviral treatment. *Expert Opin Drug Saf* 18: 829–840, 2019. doi:10.1080/14740338.2019.1644317.
35. **Lovejoy JC**, **Champagne CM**, **de Jonge L**, **Xie H**, **Smith SR.** Increased visceral fat and decreased energy expenditure during the menopausal transition. *Int J Obes* 32: 949–958, 2008. doi:10.1038/ijo.2008.25.
36. **Ferrara CM**, **Lynch NA**, **Nicklas BJ**, **Ryan AS**, **Berman DM.** Differences in adipose tissue metabolism between postmenopausal and perimenopausal women. *J Clin Endocrinol Metab* 87: 4166–4170, 2002. doi:10.1210/jc.2001-012034.
37. **Yamatani H**, **Takahashi K**, **Yoshida T**, **Soga T**, **Kurachi H.** Differences in the fatty acid metabolism of visceral adipose tissue in postmenopausal women. *Menopause* 21: 170–176, 2014. doi:10.1097/GME.0b013e318296431a.
38. **Chedraui P**, **Pérez-López FR**, **Escobar GS**, **Palla G**, **Montt-Guevara M**, **Cecchi E**, **Genazzani AR**, **Simoncini T**; **Research Group for the Omega Women's Health Project.** Circulating leptin, resistin, adiponectin, visfatin, adipsin and ghrelin levels and insulin resistance in postmenopausal women with and without the metabolic syndrome. *Maturitas* 79: 86–90, 2014. doi:10.1016/j.maturitas.2014.06.008.
39. **Eshtiaghi R**, **Esteghamati A**, **Nakhjavani M.** Menopause is an independent predictor of metabolic syndrome in Iranian women. *Maturitas* 65: 262–266, 2010. doi:10.1016/j.maturitas.2009.11.004.
40. **Park YW**, **Zhu S**, **Palaniappan L**, **Heshka S**, **Carnethon MR**, **Heymsfield SB.** The metabolic syndrome: prevalence and associated risk factor findings in the US population from the Third National Health and Nutrition Examination Survey, 1988-1994. *Arch Intern Med* 163: 427–436, 2003. doi:10.1001/archinte.163.4.427.
41. **Shen M**, **Kumar SP**, **Shi H.** Estradiol regulates insulin signaling and inflammation in adipose tissue. *Horm Mol Biol Clin Investig* 17: 99–107, 2014. doi:10.1515/hmbci-2014-0007.

42. **Fu Y**, **Li R**, **Zhong J**, **Fu N**, **Wei X**, **Cun X**, **Deng S**, **Li G**, **Xie J**, **Cai X**, **Lin Y.** Adipogenic differentiation potential of adipose-derived mesenchymal stem cells from ovariectomized mice. *Cell Prolif* 47: 604–614, 2014. doi:10.1111/cpr.12131.
43. **Heine PA**, **Taylor JA**, **Iwamoto GA**, **Lubahn DB**, **Cooke PS.** Increased adipose tissue in male and female estrogen receptor-alpha knockout mice. *Proc Natl Acad Sci USA* 97: 12729–12734, 2000. doi:10.1073/pnas.97.23.12729.
44. **Ford SM**, **Simon L**, **Vande Stouwe C**, **Allerton T**, **Mercante DE**, **Byerley LO**, **Dufour JP**, **Bagby GJ**, **Nelson S**, **Molina PE.** Chronic binge alcohol administration impairs glucose-insulin dynamics and decreases adiponectin in asymptomatic simian immunodeficiency virus-infected macaques. *Am J Physiol Regul Integr Comp Physiol* 311: R888–R897, 2016. doi:10.1152/ajpregu.00142.2016.
45. **Ford SM**, **Simon PL**, **Berner P**, **Cook G**, **Vande Stouwe C**, **Dufour JP**, **Bagby G**, **Nelson S**, **Molina PE.** Differential contribution of chronic binge alcohol and antiretroviral therapy to metabolic dysregulation in SIV-infected male macaques. *Am J Physiol Endocrinol Metab* 315: E892–E903, 2018. doi:10.1152/ajpendo.00175.2018.
46. **Grunfeld C**, **Rimland D**, **Gibert CL**, **Powderly WG**, **Sidney S**, **Shlipak MG**, **Bacchetti P**, **Scherzer R**, **Haffner S**, **Heymsfield SB.** Association of upper trunk and visceral adipose tissue volume with insulin resistance in control and HIV-infected subjects in the FRAM study. *J Acquir Immune Defic Syndr* 46: 283–290, 2007. doi:10.1097/QAI.0b013e31814b94e2.
47. **Wohl D**, **Scherzer R**, **Heymsfield S**, **Simberkoff M**, **Sidney S**, **Bacchetti P**, **Grunfeld C**; **FRAM Study Investigators.** The associations of regional adipose tissue with lipid and lipoprotein levels in HIV-infected men. *J Acquir Immune Defic Syndr* 48: 44–52, 2008. doi:10.1097/QAI.0b013e31816d9ba1.
48. **Srinivasa S**, **Fitch KV**, **Wong K**, **Torriani M**, **Mayhew C**, **Stanley T**, **Lo J**, **Adler GK**, **Grinspoon SK.** RAAS activation is associated with visceral adiposity and insulin resistance among HIV-infected patients. *J Clin Endocrinol Metab* 100: 2873–2882, 2015. doi:10.1210/jc.2015-1461.
49. **Stanley TL**, **Falutz J**, **Marsolais C**, **Morin J**, **Soulban G**, **Mamputu JC**, **Assaad H**, **Turner R**, **Grinspoon SK.** Reduction in visceral adiposity is associated with an improved metabolic profile in HIV-infected patients receiving tesamorelin. *Clin Infect Dis* 54: 1642–1651, 2012. doi:10.1093/cid/cis251.
50. **Scherzer R**, **Heymsfield SB**, **Lee D**, **Powderly WG**, **Tien PC**, **Bacchetti P**, **Shlipak MG**, **Grunfeld C**; **Study of Fat Redistribution and Metabolic Change in HIV Infection (FRAM).** Decreased limb muscle and increased central adiposity are associated with 5-year all-cause mortality in HIV infection. *AIDS* 25: 1405–1414, 2011. doi:10.1097/QAD.0b013e32834884e6.
51. **Dodd T**, **Simon L**, **LeCapitaine NJ**, **Zabaleta J**, **Mussell J**, **Berner P**, **Ford S**, **Dufour J**, **Bagby GJ**, **Nelson S**, **Molina PE.** Chronic binge alcohol administration accentuates expression of pro-fibrotic and inflammatory genes in the skeletal muscle of simian immunodeficiency virus-infected macaques. *Alcohol Clin Exp Res* 38: 2697–2706, 2014. doi:10.1111/acer.12545.
52. **LeCapitaine NJ**, **Wang ZQ**, **Dufour JP**, **Potter BJ**, **Bagby GJ**, **Nelson S**, **Cefalu WT**, **Molina PE.** Disrupted anabolic and catabolic processes may contribute to alcohol-accentuated SAIDS-associated wasting. *J Infect Dis* 204: 1246–1255, 2011. doi:10.1093/infdis/jir508.
53. **Molina PE**, **Lang CH**, **McNurlan M**, **Bagby GJ**, **Nelson S.** Chronic alcohol accentuates simian acquired immunodeficiency syndrome-associated wasting. *Alcohol Clin Exp Res* 32: 138–147, 2008. doi:10.1111/j.1530-0277.2007.00549.x.
54. **Molina PE**, **Amedee AM**, **Veazey R**, **Dufour J**, **Volaufova J**, **Bagby GJ**, **Nelson S.** Chronic binge alcohol consumption does not diminish effectiveness of continuous antiretroviral suppression of viral load in simian immunodeficiency virus-infected macaques. *Alcohol Clin Exp Res* 38: 2335–2344, 2014. doi:10.1111/acer.12507.
55. **Simon L**, **Siggins R**, **Winsauer P**, **Brashear M**, **Ferguson T**, **Mercante D**, **Song K**, **Vande Stouwe C**, **Nelson S**, **Bagby G**, **Amedee A**, **Molina PE.** Simian immunodeficiency virus infection increases blood ethanol concentration duration after both acute and chronic administration. *AIDS Res Hum Retroviruses* 34: 178–184, 2018. doi:10.1089/AID.2017.0195.
56. **Yang F**, **Shen Y**, **Camp DG**, **Smith RD.** High-pH reversed-phase chromatography with fraction concatenation for 2D proteomic analysis. *Expert Rev Proteomics* 9: 129–134, 2012. doi:10.1586/epr.12.15.
57. **Pascale CL**, **Martinez AN**, **Carr C**, **Sawyer DM**, **Ribeiro-Alves M**, **Chen M**, **O'Donnell DB**, **Guidry JJ**, **Amenta PS**, **Dumont AS.** Treatment with dimethyl fumarate reduces the formation and rupture of intracranial aneurysms: role of Nrf2 activation. *J Cereb Blood Flow Metab* 40: 1077–1089, 2020. doi:10.1177/0271678X19858888.
58. **Yue X**, **Guidry JJ.** Differential protein expression profiles of bronchoalveolar lavage fluid following lipopolysaccharide-induced direct and indirect lung injury in mice. *Int J Mol Sci* 20: 3401, 2019. doi:10.3390/ijms20143401.
59. **Filipeanu CM**, **Pullikuth AK**, **Guidry JJ.** Molecular determinants of the human α2C-adrenergic receptor temperature-sensitive intracellular traffic. *Mol Pharmacol* 87: 792–802, 2015. doi:10.1124/mol.114.096198.
60. **Harman JC**, **Guidry JJ**, **Gidday JM.** Intermittent hypoxia promotes functional neuroprotection from retinal ischemia in untreated first-generation offspring: proteomic mechanistic insights. *Invest Ophthalmol Vis Sci* 61: 15, 2020. doi:10.1167/iovs.61.11.15.
61. **Orsburn BC.** Proteome discoverer: a community enhanced data processing suite for protein informatics. *Proteomes* 9: 15, 2021. doi:10.3390/proteomes9010015.
62. **Tabb DL**, **Eng JK**, **Yates JR.** Protein identification by SEQUEST. In: *Proteome Research: Mass Spectrometry*. Berlin, Heidelberg: Springer, 2001, p. 125–142.
63. **Vizcaíno JA**, **Deutsch EW**, **Wang R**, **Csordas A**, **Reisinger F**, **Ríos D**, **Dianes JA**, **Sun Z**, **Farrah T**, **Bandeira N**, **Binz PA**, **Xenarios I**, **Eisenacher M**, **Mayer G**, **Gatto L**, **Campos A**, **Chalkley RJ**, **Kraus HJ**, **Albar JP**, **Martinez-Bartolomé S**, **Apweiler R**, **Omenn GS**, **Martens L**, **Jones AR**, **Hermjakob H.** ProteomeXchange provides globally coordinated proteomics data submission and dissemination. *Nat Biotechnol* 32: 223–226, 2014. doi:10.1038/nbt.2839.
64. **Vizcaíno JA**, **Csordas A**, **Del-Toro N**, **Dianes JA**, **Griss J**, **Lavidas I**, **Mayer G**, **Perez-Riverol Y**, **Reisinger F**, **Ternent T**, **Xu QW**, **Wang R**, **Hermjakob H.** 2016 update of the PRIDE database and its related tools. *Nucleic Acids Res* 44: 11033, 2016. doi:10.1093/nar/gkw880.
65. **Krämer A**, **Green J**, **Pollard J**, **Tugendreich S.** Causal analysis approaches in Ingenuity Pathway Analysis. *Bioinformatics* 30: 523–530, 2014. doi:10.1093/bioinformatics/btt703.
66. **Kema VH**, **Mojerla NR**, **Khan I**, **Mandal P.** Effect of alcohol on adipose tissue: a review on ethanol mediated adipose tissue injury. *Adipocyte* 4: 225–231, 2015. doi:10.1080/21623945.2015.1017170.
67. **Parker R**, **Kim SJ**, **Gao B.** Alcohol, adipose tissue and liver disease: mechanistic links and clinical considerations. *Nat Rev Gastroenterol Hepatol* 15: 50–59, 2018. doi:10.1038/nrgastro.2017.116.
68. **Sebastian BM**, **Roychowdhury S**, **Tang H**, **Hillian AD**, **Feldstein AE**, **Stahl GL**, **Takahashi K**, **Nagy LE.** Identification of a cytochrome P4502E1/Bid/C1q-dependent axis mediating inflammation in adipose tissue after chronic ethanol feeding to mice. *J Biol Chem* 286: 35989–35997, 2011. doi:10.1074/jbc.M111.254201.
69. **Tang H**, **Sebastian BM**, **Axhemi A**, **Chen X**, **Hillian AD**, **Jacobsen DW**, **Nagy LE.** Ethanol-induced oxidative stress via the CYP2E1 pathway disrupts adiponectin secretion from adipocytes. *Alcohol Clin Exp Res* 36: 214–222, 2012. doi:10.1111/j.1530-0277.2011.01607.x.
70. **Bagby GJ**, **Zhang P**, **Purcell JE**, **Didier PJ**, **Nelson S.** Chronic binge ethanol consumption accelerates progression of simian immunodeficiency virus disease. *Alcohol Clin Exp Res* 30: 1781–1790, 2006. doi:10.1111/j.1530-0277.2006.00211.x.
71. **Nanji AA**, **Hiller-Sturmhöfel S.** Apoptosis and necrosis: two types of cell death in alcoholic liver disease. *Alcohol Health Res World* 21: 325–330, 1997.
72. **Ambade A**, **Mandrekar P.** Oxidative stress and inflammation: essential partners in alcoholic liver disease. *Int J Hepatol* 2012: 853175, 2012. doi:10.1155/2012/853175.
73. **Das SK**, **Vasudevan DM.** Alcohol-induced oxidative stress. *Life Sci* 81: 177–187, 2007. doi:10.1016/j.lfs.2007.05.005.
74. **Duplanty AA**, **Simon L**, **Molina PE.** Chronic binge alcohol-induced dysregulation of mitochondrial-related genes in skeletal muscle of simian immunodeficiency virus-infected rhesus macaques at end-stage disease. *Alcohol Alcohol* 52: 298–304, 2017. doi:10.1093/alcalc/agw107.
75. **Yin M**, **Ikejima K**, **Wheeler MD**, **Bradford BU**, **Seabra V**, **Forman DT**, **Sato N**, **Thurman RG.** Estrogen is involved in early alcohol-induced liver injury in a rat enteral feeding model. *Hepatology* 31: 117–123, 2000. doi:10.1002/hep.510310119.

76. **Carr MC.** The emergence of the metabolic syndrome with menopause. *J Clin Endocrinol Metab* 88: 2404–2411, 2003. doi:10.1210/jc.2003-030242.
77. **Looby SE.** Menopause-associated metabolic manifestations and symptomatology in HIV infection: a brief review with research implications. *J Assoc Nurses AIDS Care* 23: 195–203, 2012. doi:10.1016/j.jana.2011.06.008.
78. **Wang Q**, **Ferreira DLS**, **Nelson SM**, **Sattar N**, **Ala-Korpela M**, **Lawlor DA.** Metabolic characterization of menopause: cross-sectional and longitudinal evidence. *BMC Med* 16: 17, 2018. doi:10.1186/s12916-018-1008-8.
79. **Sears S**, **Buendia JR**, **Odem S**, **Qobadi M**, **Wortley P**, **Mgbere O**, **Sanders J**, **Spencer EC**, **Barnes A.** Metabolic syndrome among people living with HIV receiving medical care in Southern United States: prevalence and risk factors. *AIDS Behav* 23: 2916–2925, 2019. doi:10.1007/s10461-019-02487-8.
80. **Warriner AH**, **Burkholder GA**, **Overton ET.** HIV-related metabolic comorbidities in the current ART era. *Infect Dis Clin North Am* 28: 457–476, 2014. doi:10.1016/j.idc.2014.05.003.
81. **Blüher M.** Importance of estrogen receptors in adipose tissue function. *Mol Metab* 2: 130–132, 2013. doi:10.1016/j.molmet.2013.07.001.
82. **Kanapathipillai R**, **Hickey M**, **Giles M.** Human immunodeficiency virus and menopause. *Menopause* 20: 983–990, 2013. doi:10.1097/GME.0b013e318282aa57.
83. **Helguero LA**, **Faulds MH**, **Gustafsson JA**, **Haldosén LA.** Estrogen receptors alfa (ERalpha) and beta (ERbeta) differentially regulate proliferation and apoptosis of the normal murine mammary epithelial cell line HC11. *Oncogene* 24: 6605–6616, 2005. doi:10.1038/sj.onc.1208807.
84. **Kim JK**, **Pedram A**, **Razandi M**, **Levin ER.** Estrogen prevents cardiomyocyte apoptosis through inhibition of reactive oxygen species and differential regulation of p38 kinase isoforms. *J Biol Chem* 281: 6760–6767, 2006. doi:10.1074/jbc.M511024200.
85. **Lewis-Wambi JS**, **Jordan VC.** Estrogen regulation of apoptosis: how can one hormone stimulate and inhibit? *Breast Cancer Res* 11: 206, 2009. doi:10.1186/bcr2255.
86. **Spyridopoulos I**, **Sullivan AB**, **Kearney M**, **Isner JM**, **Losordo DW.** Estrogen-receptor-mediated inhibition of human endothelial cell apoptosis. Estradiol as a survival factor. *Circulation* 95: 1505–1514, 1997. doi:10.1161/01.cir.95.6.1505.
87. **Gompel A**, **Somaï S**, **Chaouat M**, **Kazem A**, **Kloosterboer HJ**, **Beusman I**, **Forgez P**, **Mimoun M**, **Rostène W.** Hormonal regulation of apoptosis in breast cells and tissues. *Steroids* 65: 593–598, 2000. doi:10.1016/s0039-128x(00)00172-0.